LEGIBILITY NOTICE

A major purpose of the Technical Information Center is to provide the broadest dissemination possible of information contained in DOE's Research and Development Reports to business, industry, the academic community, and federal, state and local governments.

Although a small portion of this report is not reproducible, it is being made available to expedite the availability of information on the research discussed herein.

LA-UR--88-3167

DE89 000355

Los Alamos National Laboratory is operated by the University of California for the United States Department of Energy under contract W-7405-ENG-36

TITLE A STEREOLOGICAL ANALYSIS OF DUCTILE FRACTURE BY MICROVOID COALESCENCE

AUTHOR(S) J(ames) H. Steele, Jr.

SUBMITTED TO 7th International Conference on Fracture

DISCLAIMER

MASTER

Los Alamos National Laboratory
Los Alamos, New Mexico 87545

A Stereological Analysis of Ductile Fracture by Microvoid Coalescence

By: James H. Steele Jr., Los Alamos National Laboratory
Los Alamos, New Mexico, 87545

ABSTRACT

A stereological analysis for ductile fracture by microvoid coalescence is presented based upon the model of Widgery and Knott which postulates that microvoids link with a propagating crack if they lie within a certain interaction distance of its plane. A 3-dimensional analytical expression for dimple density and shape is developed from this model using projected image relationships for a thin slab. Void nucleation and growth are incorporated into the analysis using numerical integration of the Rice-Tracey growth equation over the appropriate strain range. The parameters required for application of the analysis include; number per unit volume and volume fraction of nucleating particles, the fraction of particles nucleating voids, a nucleation model or measured data for nucleation rate as a function of plastic strain, the fracture strain, the interaction distance for microvoid coalescence, and the stress and strain conditions involved in the test. An evaluation of the stereological approach is given using tensile data from a spheroidized 1045 steel to predict the effect of hydrostatic pressure upon the dimple density. The analysis, which is consistent with observed correlations between dimple density and second phase particle density, is shown to provide an estimates of dimple size and the microroughness parameter used in local stain models for microvoid coalescence.

INTRODUCTION

The ductility and fracture toughness of a majority of engineering alloys which fail by microvoid coalescence (MVC) are controlled by the dispersion of second phase particles. This is a consequence of the nucleation and growth of microvoids at particles during plastic deformation. These local damage processes, which are statistical in nature, continue until some type of instability or flow localization process intervenes to produce a macroscopic crack or fracture. The most common instability involves the linking of nearest neighbor microvoids by necking of the intervening matrix regions.[1,2] Its occurrence is associated with the change from macroscopic plastic flow to localized deformation within a thin layer which forms the final dimpled fracture surface. Experimental observations have clearly established that such ductile fracture surfaces are produced by a sudden intense localized necking of the intervoid matrix across a sheet of microvoids. Thus MVC is confined almost exclusively to a thin layer adjacent to the final fracture surface as observed experimentally[3]. The three-dimensional model described by Thomason[4,5] for necking instability within the intervoid matrix of a simple cubic array of monosize spherical voids emphasizes the complexity of the problem of establishing the conditions that lead to its onset. Unfortunately the a priori stereological assumptions do not allow dispersion effects such as a range of nucleation strains, and the size and spatial distribution of microvoids, to be included. It also appears that current dilatant plasticity models[6,7] for ductile fracture via MVC do not furnish realistic predictions of void volume fractions of 4-5% as observed at the onset of coalescence.[8,9] In addition none of the current models provide estimates or predictions for dimple sizes and the shapes

expected on the fracture surface, nor do they provide a basis for understanding the linear correlation observed between planar particle density and dimple density.[10,11]

The stereological approach presented in this paper is based upon the geometric model proposed by Widgery and Knott[12], wherein void coalescence occurs within a thin volume element whose thickness corresponds to a physical interaction distance required for microvoid coalescence. Hence necking instability is confined to the continuous three dimensional intervoid matrix separating nearest neighbor voids within the volume element bounded by the interaction distance. This condition gives a unique definition for the microstructural size scale involved in void coalescence, and thus it may furnish a characteristic length, as discussed by Rice[13], needed for relating microstructure and fracture parameters. The interaction distance postulated by this model does not represent an a priori definition for the critical condition or conditions necessary for the instability. It does, however, define a characteristic length that is controlled by those conditions which are necessary and sufficient for onset of the necking instability. The advantage of this approach lies in the ability to measure interaction distance[12], and thereby provide a rational basis for evaluating and understanding the critical conditions. Application of this geometric model for evaluating the physical and microstructural factors that are involved in the coalescence process and in controlling dimple size and shape will be described in this paper.

Stereological Model for Microvoid Coalescence

The geometric model for coalescence within a thin volume element, with thickness t equal to the interaction distance, furnishes the following projected image relationship[14] between void density,

N_V, and expected dimple density, $\langle N_A \rangle$, on the fracture surface,

$$\langle N_A(\text{dimples}) \rangle = N_V(\text{voids}) \{ \langle D_C(\text{voids}) \rangle + t \} \qquad ..(1)$$

This equation is based upon a thin section through a random dispersion of convex microvoids with average caliper diameter, $\langle D_C \rangle$, normal to the section, as illustrated in Figure 1. Physically the relationship confines the necking instability to the intervoid matrix prescribed by nearest neighbor voids within the planar interaction volume. Hence the coalescence process is limited to a statistical sheet of microvoids as suggested by other models[5], and as observed experimentally[3]. Projected void density at the onset of instability is therefore equal to the expected dimple density on the fracture surface. This is illustrated schematically in Figure 2 which shows a projected view of voids contained within a thin section with their nearest neighbor regions delineated by Dirichlet cells[15]. The instability is thus envisioned as the three dimensional physical process that creates continuous knife-edge ridges, classically observed on ductile fracture surfaces, by necking along the Dirichlet cell boundaries.

Equation (1) can be expressed in terms of particle density, $N_V(p)$, and a dimensionless thickness, k, by defining,

$$N_V(v) = f_n * N_V(p)$$

$$k = t / \langle D_C(v) \rangle$$

where f_n is the fraction of particles that nucleate voids. Thus expected dimple density is given as a simple product of physical and microstructural parameters as,

$$\langle N_A(\text{dimples}) \rangle = f_n * N_V(p) * \langle D_C(v) \rangle * (k + 1) \qquad ..(2)$$

The stereological assumptions involved in this relationship are a thin volume sampling of the void dispersion, and convex void shapes. The physical conditions implicit in equation (2) are: that necking

instability is constrained within the planar volume element, that t is controlled by the critical conditions for instability which are unspecified in this model, and that f_n does not change during coalescence. Application of equation (2) to predict dimple size requires stereological estimation of $N_V(p)$, $\langle D_C(v) \rangle$, k, and f_n, which involve size distribution, and/or three dimensional sampling techniques[16]. Hence values for these parameters are not available in studies on ductile fracture, and a nucleation and growth model must be employed to allow application of equation (2) to experimental data.

The most important, and the most difficult parameter to measure in equation (2) is the average microvoid size, $\langle D_C(v) \rangle$, normal to the fracture surface. This parameter has been employed to describe the critical damage condition for void coalescence[17], and it is also the principal microstructural factor in local strain models of ductile fracture[18]. Evaluation of $\langle D_C \rangle$ requires that void nucleation and growth be either modeled, or measured over the stress-strain path for a specific test. The stereological approach is equivalent to the growth path analysis of DeHoff[19], as illustrated in Figure 3, where microstructural evolution involves the local damage processes of void nucleation and growth which are a function of strain path rather than time. Application of the growth path analysis thus requires that void size distributions be measured over the strain path of a specific test. As void size distributions have not been measured for tensile tests, equation (2) will be applied using the classic Rice-Tracey[20] growth model and the assumption that the nucleation rate is a constant.

The Rice-Tracey growth model for evolution of noninteracting spherical voids in a remote triaxial stress field has been applied in several recent papers[3,7,8]. Principal radii for the axially symmetric ellipsoidal voids that grow under remote tensile stress conditions are given by,

$$R3(\epsilon f,\epsilon n,\sigma m/\sigma e) = R0\exp\left(\int_{\epsilon n}^{\epsilon f}(\gamma(\sigma m/\sigma e) + D(\sigma m/\sigma e))\, d\epsilon\right) \quad ..(3)$$

$$R1(\epsilon f,\epsilon n,\sigma m/\sigma e) = R0\exp\left(\int_{\epsilon n}^{\epsilon f}(-\gamma(\sigma m/\sigma e)/2 + D(\sigma m/\sigma e))\, d\epsilon\right) \quad ..(4)$$

Where R0 = initial void size, ϵf = fracture strain, ϵn = nucleation strain, γ = shape change function, D = dilatational function, and $\sigma m/\sigma e$ = mean stress/effective stress. R3 defines the void size in the direction of principal tensile stress and thus $2R3 = D_c$. R1 is the void size normal to the direction of principal tensile stress. R0, the initial spherical void size, will be assumed to be equal to the size of the nucleating particle which implies that the physical mechanism for void nucleation is interface decohesion. In addition R0 may depend on strain if particle size affects the void nucleation conditions. These equations can be used to calculate growth paths for individual voids when the stress state can be expressed as a function of effective plastic strain. The data of BrownRigg et al[8], which provide analytic expressions for the stress state during tensile testing, will be used for illustration. This is convenient since their data also provide dimple size measurements to which the model will be compared in the next section. Figure 4 shows the mean and effective stress as a function of plastic strain for necking of their round 1045 steel tensile specimens. The functions $\gamma(\epsilon)$ and $D(\epsilon)$ are shown in Figure 5 along with plots of their values for the tensile stress conditions shown in Figure 4. The effect of hydrostatic pressure in reducing the dilatational function is clearly shown by these data.

Growth paths for voids that nucleate at different plastic strains can be readily calculated by numerical integration of these equations over the strain interval between nucleation and fracture. Figure 6 shows calculated growth paths for voids that nucleate at different strain levels. These results illustrate the effect of triaxial stress state in increasing void growth rate in the direction of principal tensile stress. In addition they indicate that voids tend to shrink in the R1 direction rather than grow as suggested by BrownRigg et al.[8] The dependence of R3 on nucleation strain illustrates the necessity for either a stereological analysis or a model for nucleation rate to establish the appropriate average for D_C. This is also indicated by experimental studies[9,21], which show that nucleation exhibits a statistical dispersion over a significant range of plastic strain.

Void nucleation frequency may be expressed as a distribution function normalized over the strain interval of the test as,

$$F(x) = \int_0^x f(\epsilon)d\epsilon = \text{fraction nucleated for } \epsilon < x$$

where $f(\epsilon)d\epsilon$ is the fraction of voids nucleated in the strain interval ϵ to $\epsilon+d\epsilon$. The average for D_C can thus be expressed as,

$$\langle D_C(\text{voids})\rangle = 2\langle R3\rangle = 2\int_0^{\epsilon_f} f(\epsilon)*R3(\epsilon f,\epsilon,\sigma_m/\sigma_e)\ d\epsilon \qquad ..(5)$$

The simplest model for nucleation involves a constant nucleation rate with a starting strain, ϵs, and ending strain, ϵe. This nucleation model, which was employed by LeRoy et al[3] for similar tensile tests, gives an average value for R3 as,

$$\langle R3\rangle = \{1/(\epsilon e-\epsilon s)\}\int_{\epsilon s}^{\epsilon e} R3(\epsilon f,\epsilon,\sigma_m/\sigma_e)\ d\epsilon \qquad ..(6)$$

This equation allows <R3> to be calculated by numerical integration after substitution of the Rice-Tracey growth function in equation (3). Although other distribution functions can be used for nucleation rate, such as the Gaussian function applied by Tvergaard and Needleman[7],

available data are not sufficient to identify the functional form needed to represent the nucleation process. It is important to recognize that a void nucleation and growth model will permit the calculation of expected volume fraction, V_V, and other parameters which characterize the damage process as a function of strain.

APPLICATION OF THE MODEL

This section gives the results of application of the model to experimental data reported on tensile tests of spheroidized 1045 steel with varying hydrostatic pressure[8]. Microstructural, fractographic, and test parameters reported for material with a coarse carbide dispersion are presented in Table I. The estimated value for carbide density was selected to be consistent with the largest experimental planar void densities measured. The strain corresponding to the start of nucleation was selected to indicate the beginning of the more profuse nucleation of voids at carbides. This is consistent with the suggestion[3] that two populations, inclusions and carbides, may be responsible for the observed damage evolution process. Thus void volume fraction can be calculated using the Rice-Tracey growth model and a constant nucleation rate from the stereological relationship,

$$V_V(\text{voids}) = N_V(\text{voids}) * \langle \text{Volume} \rangle$$

where $\langle \text{Volume} \rangle = (4\pi/3) * \langle R3 \rangle * \langle R1 \rangle^2$, since R_1 is approximately constant as indicated by the growth data in Figure 6. Calculated void volume fractions are presented in Figure 7, along with the experimental area fraction data. Void fractions calculated by subtracting the volume of nucleating carbides show an excellent fit to the stereological measurements for each hydrostatic pressure. The appropriate V_V for comparison clearly should not involve the volume of nucleating carbides since they were not included in the experimental void fraction data.

The average value, $\langle D_c(\text{voids})\rangle$, was obtained by numerical integration of equation (6) for the strain ranges indicated in Table I. This allowed the expected dimple density to be estimated for the selected values of k and f_n. It may appear that these are arbitrary parameters in the model, however, this is only because their values were not measured by BrownRigg et al[8]. The values selected for f_n and R0 were based upon the experimental data reported by Argon and Im[21] on 1045 steel with a small adjustment to match the largest experimental volume fraction levels. The value k=1 was selected as a first approximation based upon the Brown and Embury[17] model for coalescence. The expected dimple density obtained from equation (2), thus provided an average dimple size from,

$$D_p = 1.13/\sqrt{\langle N_A \rangle}$$

which gives the equivalent circle size for the average projected dimple area. Calculated dimple sizes are plotted in Figure 8 as a function of hydrostatic pressure for comparison with fractographic measurements. The comparison between calculated and experimental dimple sizes is excellent even though the measured data were not corrected for nonplanar topography of the fracture surface[22], which may increase their values by as much as 50%.

$\langle R3\rangle$ and $\langle D_p\rangle$ can be used to estimate the microroughness defined by Thompson and Ashby[18] as, $M = \langle R3\rangle/\langle D_p\rangle$. Although experimental measurements are not available for comparison the trend does follow that suggested by the highly elongated voids observed with increasing hydrostatic pressure. Calculated values for $\langle R3\rangle$ and M are also plotted in Figure 8 for comparison with the dimple size data.

DISCUSSION

The results for volume fraction evolution and dimple size variation with pressure indicate that the stereological model applied for constant nucleation rate with the Rice-Tracey growth equations provides an excellent description of the ductile fracture process and MVC for tensile test conditions. The classic overestimate of fracture strain by the Rice-Tracey growth model[20] thus appears to be the result of the requirement that coalescence occur by lateral void growth until impingement rather than the need to incorporate the effect of dilatant matrix plasticity.[7] This model is therefore consistent with Thomason's model[4,5] that necking (load-limit) instability intervenes to cause MVC before dilatant plasticity of the porous matrix plays any role in the coalescence mechanism. Also it would appear that local impingement by the joining of closely spaced void pairs discussed by Thompson[23] has little if any effect on the necking instability that produces this type of void coalescence.

The stereological model does not specify critical conditions for the necking instability, but rather it indicates how one can evaluate these conditions by exploiting appropriate stereological section and fractographic measurements. As an example equation (2) shows that k can be estimated from the dimple density and $\langle N_A(\text{voids})\rangle$ normal to the tensile axis since it can be written as,

$$\langle N_A(\text{dimples})\rangle = \langle N_A(\text{voids})\rangle * (k + 1) \qquad ..(7)$$

The value of t can thus be estimated where $\langle D_C(\text{voids})\rangle$ normal to the tensile axis is measured stereologically. This again illustrates the importance of estimating average void size normal to the tensile axis in studying ductile fracture. One method for estimating $\langle D_C(\text{voids})\rangle$ is to assume that the voids are ellipsoids of

revolution as in the Rice-Tracey growth model and apply the method described by DeHoff[24] which is illustrated in Figure 10. This method gives the N_V(voids) as well as <R1> and <R3> and thus provides both the nucleation and growth paths if applied over the strain path. This result emphasizes the need to apply appropriate stereological methods for characterizing the void nucleation and growth paths in order to understand the ductile fracture process and the critical conditions for MVC.

REFERENCES

1. A. H. Cottrell, Fracture, ed. B. L. Averbach et al, Wiley, N. Y., 1959, p. 20-44.
2. P. F. Thomason, J. Inst. Metals, Vol. 96(1968), p. 360-365.
3. G. LeRoy, J. D. Embury, G. Edward, and M. F. Ashby, Acta Metall., Vol. 29(1981), p. 1509-1522.
4. P. F. Thomason, Acta Metall., Vol. 33(1985), pp. 1079-1085.
5. P. F. Thomason, Acta Metall., Vol. 33(1985), pp. 1087-1095.
6. A. L. Gurson, J. Engng. Mat. Tech., Vol. 99(1977), pp. 2-15.
7. V. Tvergaard and A. Needleman, Acta. Metall., Vol. 32(1984), pp. 157-169.
8. A. BrownRigg, W. A. Spitzig, O. Richmond, D. Tierlinck, and J. D. Embury, Acta Metall., Vol. 31(1983), pp. 1141-1150.
9. R. D. Thomson, and J. W. Hancock, Int J. Fracture, Vol. 26(1984), pp. 99-112.
10. D. Broek, Eng. Fracture Mech., Vol. 5(1973), pp. 55-66.
11. T. Inoue and S. Kinoshita, Proc 3rd Int. Conf. on Strength of Metals and Alloys, Cambridge, England, 1973, pp. 159-163.
12. D. J. Widgery and J. F. Knott, Metal Science, Vol. 12(1978), pp. 9-11.

13. J. R. Rice, The Mechanics of Fracture, ed. F. Erdogan, ASME AMD Vol 19(1976), p. 23-53.

14. J. W. Cahn and J. Nutting, Trans AIME, Vol. 215(1959), pp. 526-528.

15. P. J. Wray , O. Richmond, and H. L. Morrison, Metallography, Vol 16(1983), pp. 39-58.

16. F. N. Rhines, Microstructology: Behavior and Microstructure of Materials, Dr Riederer-Verlag, Stuttgart, 1986, p. 13.

17. L. M. Brown and J. D. Embury, Proc 3rd Int. Conf. on Strength of Metals and Alloys, Cambridge, England, 1973, pp. 164-169.

18. A. W. Thompson and M. F. Ashby, Scripta Metall., Vol. 18(1984), pp. 127-130.

19. R. T. DeHoff, Metall. Trans., Vol. 2(1971), pp. 521-526.

20. J. R. Rice and D. M. Tracey, J. Mech. Phys. Solids, Vol. 17(1969), pp. 201-217.

21. A. S. Argon and J. Im, Metall. Trans., Vol 6A(1975), pp. 839-851.

22. M. Coster and J. L. Chermant, Int. Metals Reviews, Vol. 28(1983), pp.228-250.

23. A. W. Thompson, Metall.Trans., Vol. 18A(1987), pp. 1877-1886.

24. R. T. DeHoff, Quantitative Microscopy, ed. F. N. Rhines and R. T. DeHoff, McGraw-Hill, New York, 1968, p. 143.

Microstructural Parameters for ----- BrownRigg et al
1045 Steel with Coarse Carbides Acta Met, Vol 31(1983), p 1141.

$Vv := 0.066$ = Volume Fraction Carbides

$Rx := 0.26$ = <R> from Number Distribution in μm

$Vol := 1.1$ = <Volume> Selected - in μm3

$$Nv := \frac{Vv}{Vol} \quad Nv = 0.06$$ = Calculated Number Per Unit Volume - 1/μm3

Experimental Hydrostatic Pressures = $i := 0..3$

$P_0 := 0.1$	$P_1 := 345$	$P_2 := 690$	$P_3 := 1100$	MPa
$\epsilon nu_0 := 0.3$	$\epsilon nu_1 := 0.7$	$\epsilon nu_2 := 1.1$	$\epsilon nu_3 := 1.6$	= Nucleation Start Strains.
$\epsilon fr_0 := 1.36$	$\epsilon fr_1 := 1.98$	$\epsilon fr_2 := 2.60$	$\epsilon fr_3 := 3.34$	= Fracture Strains.
$R0i_0 := 0.52$	$R0i_1 := 0.55$	$R0i_2 := 0.60$	$R0i_3 := 0.63$	= Initial Void Radius in μm.
$f_0 := 0.5$	$f_1 := 0.52$	$f_2 := 0.58$	$f_3 := 0.62$	= Fraction of Carbides Nucleating Voids.
$k_0 := 1$	$k_1 := 1$	$k_2 := 1$	$k_3 := 1$	= Interaction Thickness in μm.

TABLE I Selected experimental data used for calculations

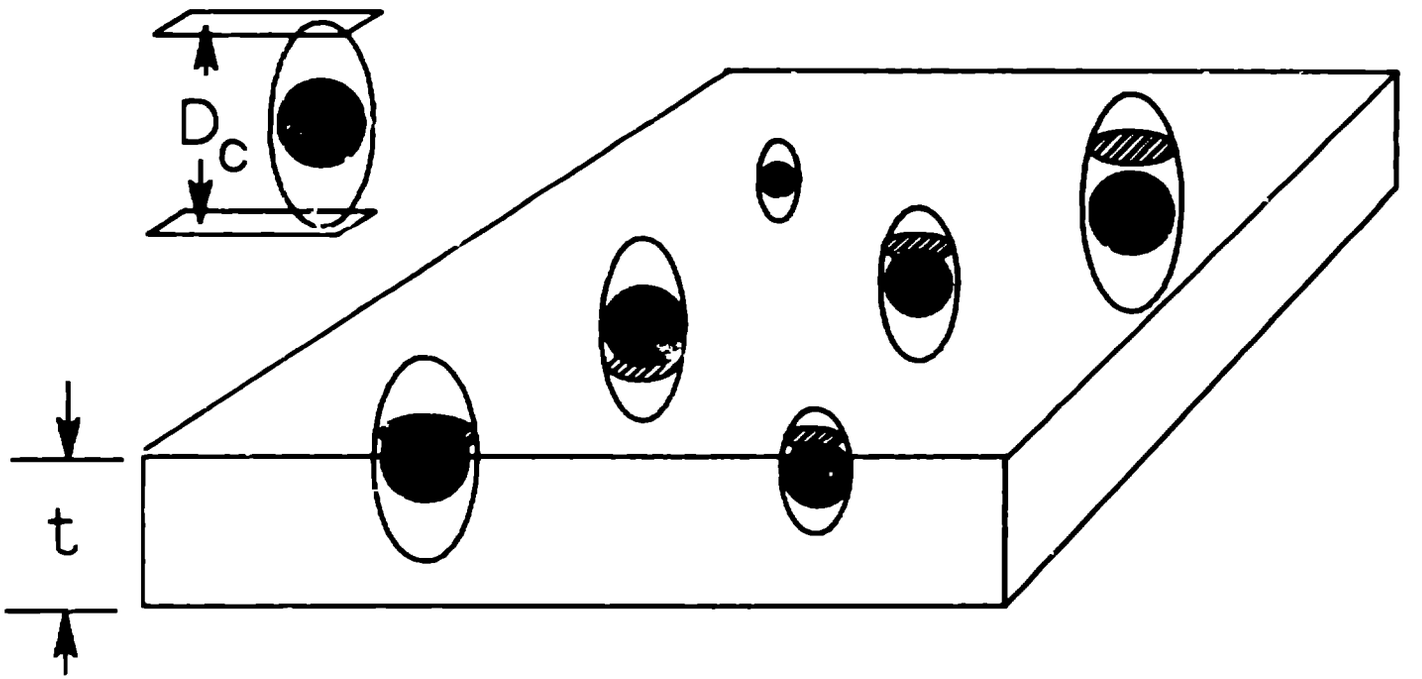

FIGURE 1 Diagram of thin section intercepting void dispersion with the Caliper Diameter, D_c , and t indicated.

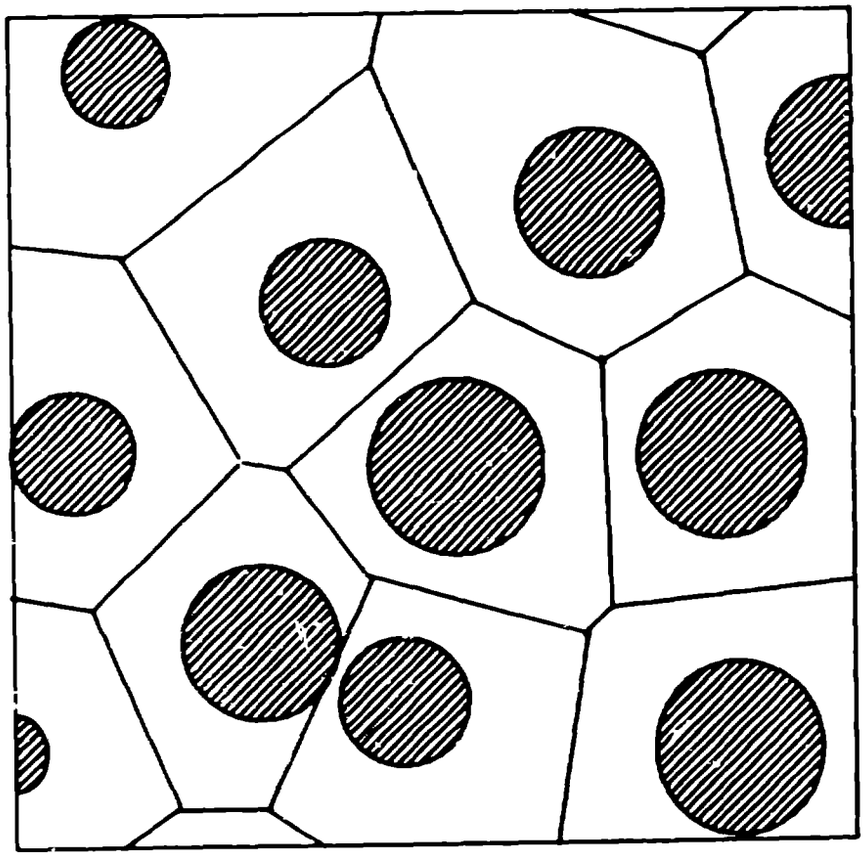

FIGURE 2 Schematic projected view void sections within the interaction volume showing nearest neighbor regions via Dirichlet cells.

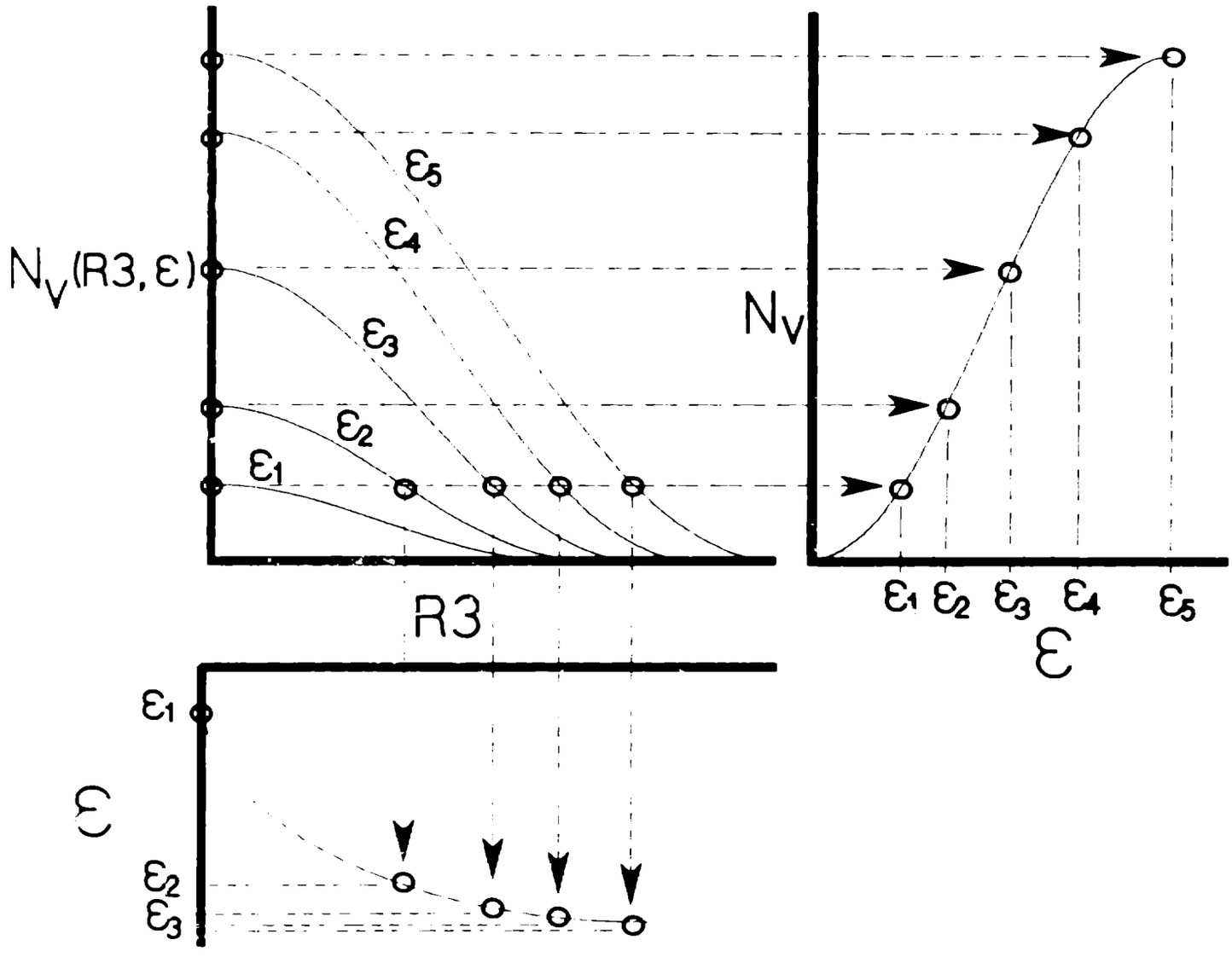

FIGURE 3 N_V Size Distribution Curves with arrows indicating Nucleation Frequency (right), and Growth Path (below)

$$\sigma m(\varepsilon, Pr) := 68 - Pr + 463 \cdot \left[1 + 57 \cdot 10^{-6} \cdot Pr\right] \cdot \varepsilon \qquad = \text{Mean Stress in MPa.}$$

$$\sigma bar(\varepsilon, Pr) := 920.0 \cdot \varepsilon^{0.25} \cdot \left[1.0 + 4.0 \cdot \frac{Pr}{G}\right] \qquad = \text{Effective Stress in MPa.}$$

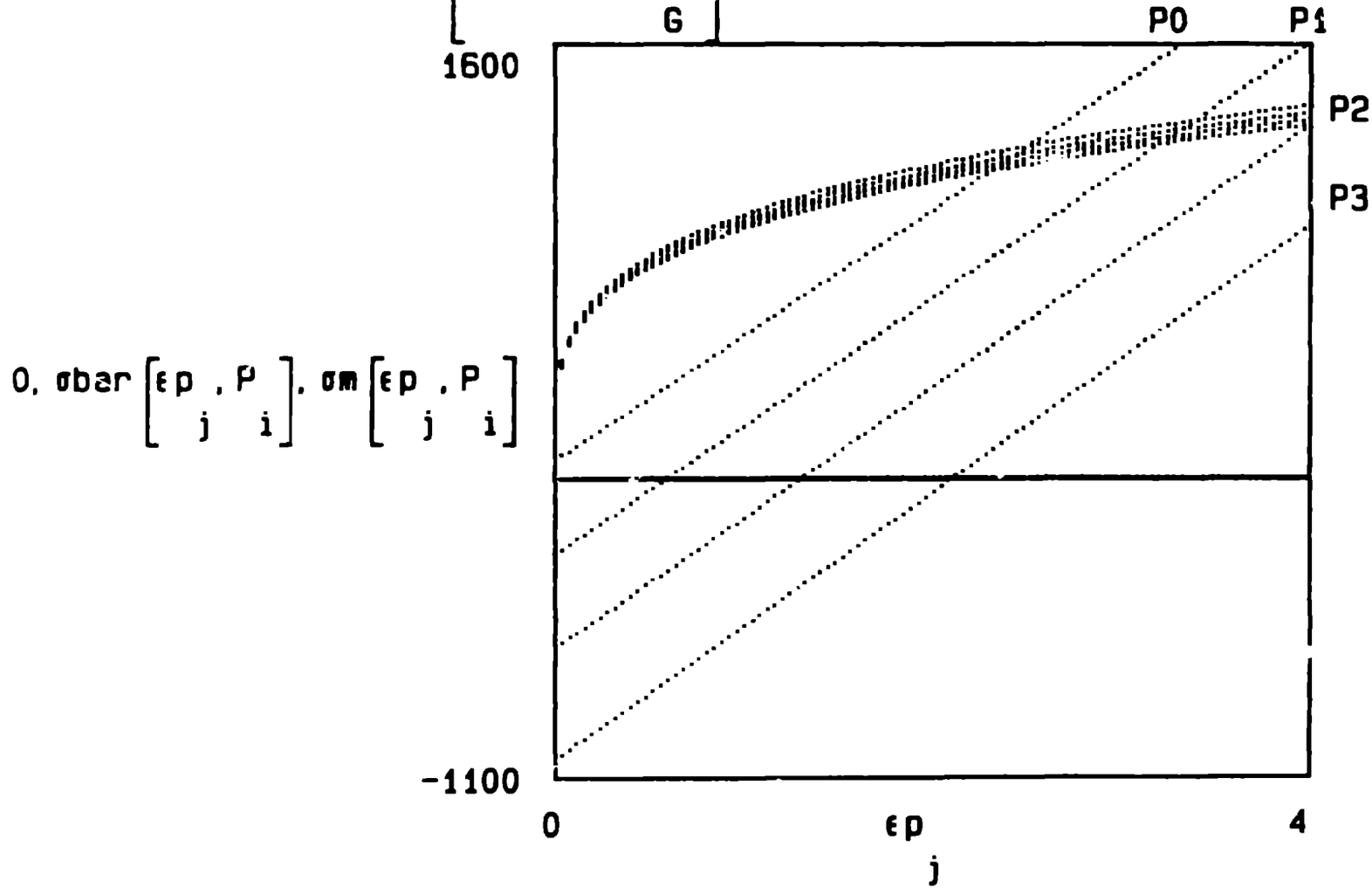

FIGURE 4 Variation of σm and σbar with strain for applied Pressure for the tensile test data of BrownRigg et al [16].

$$D(\varepsilon, Pr) := 0.558 \cdot \sinh\left[1.5 \cdot \frac{\sigma m(\varepsilon, Pr)}{\bar{\sigma}(\varepsilon, Pr)}\right] + 0.008 \cdot \cosh\left[1.5 \cdot \frac{\sigma m(\varepsilon, Pr)}{\bar{\sigma}(\varepsilon, Pr)}\right]$$

$$\bar{\sigma}(\varepsilon) := 1.67$$

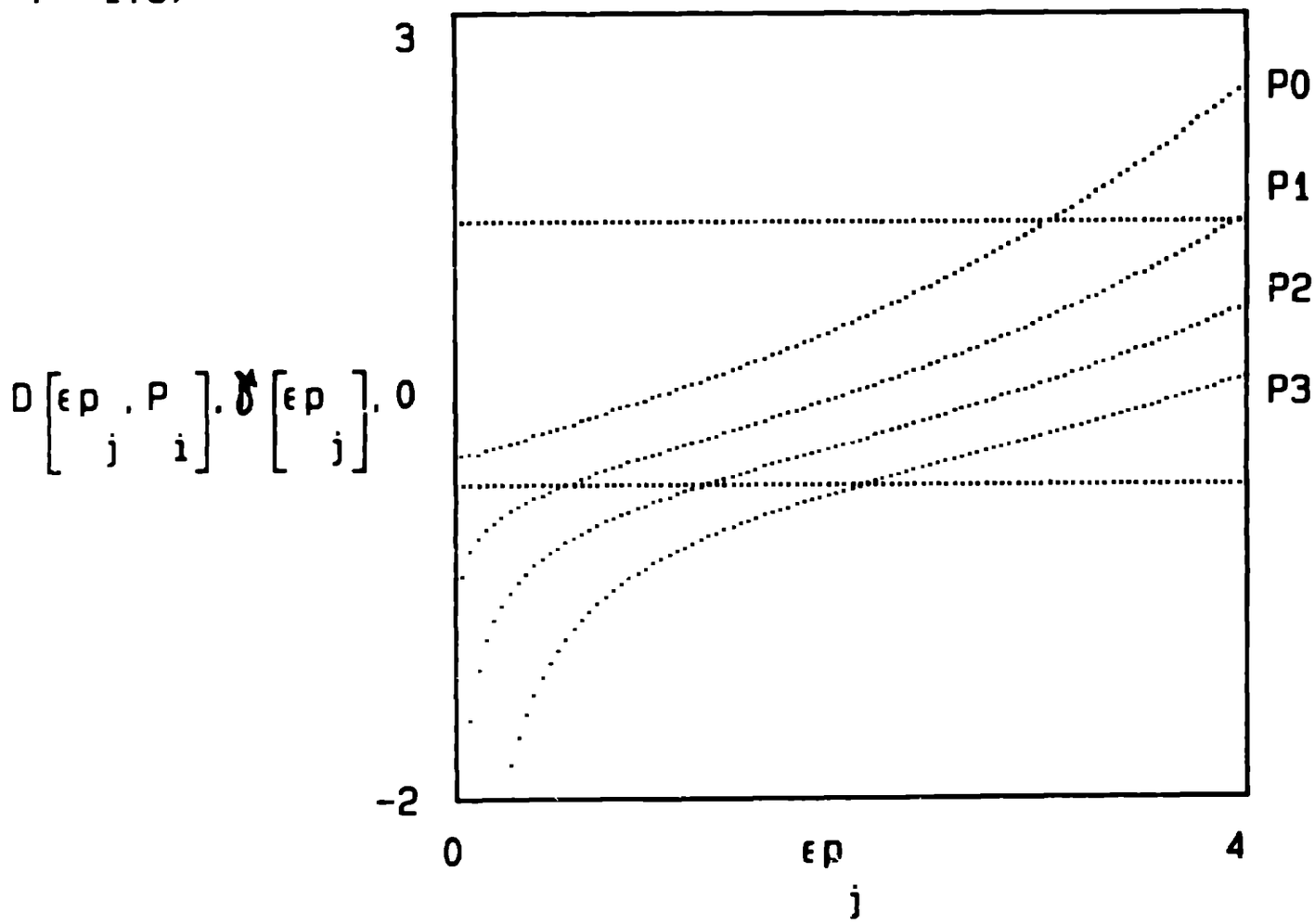

FIGURE 5 Plot of the Rice-Tracey Dilatational Function (D), and Shape Change Function ($\bar{\sigma}$) as a function of True Strain.

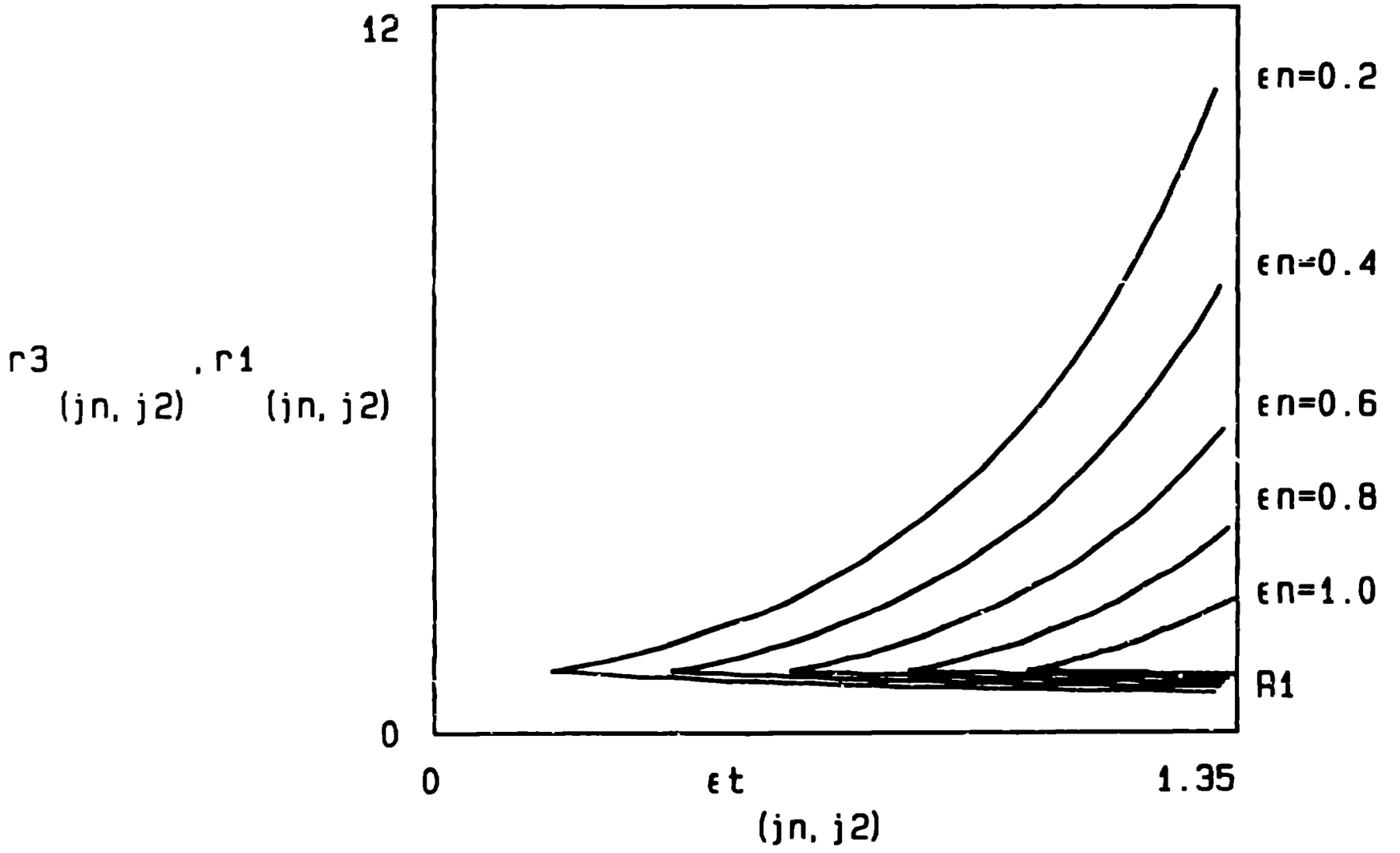

FIGURE 6 Growth Paths for Rice-Tracey Ellipsoidal Voids for Nucleation Strains indicated with P0 = 1.

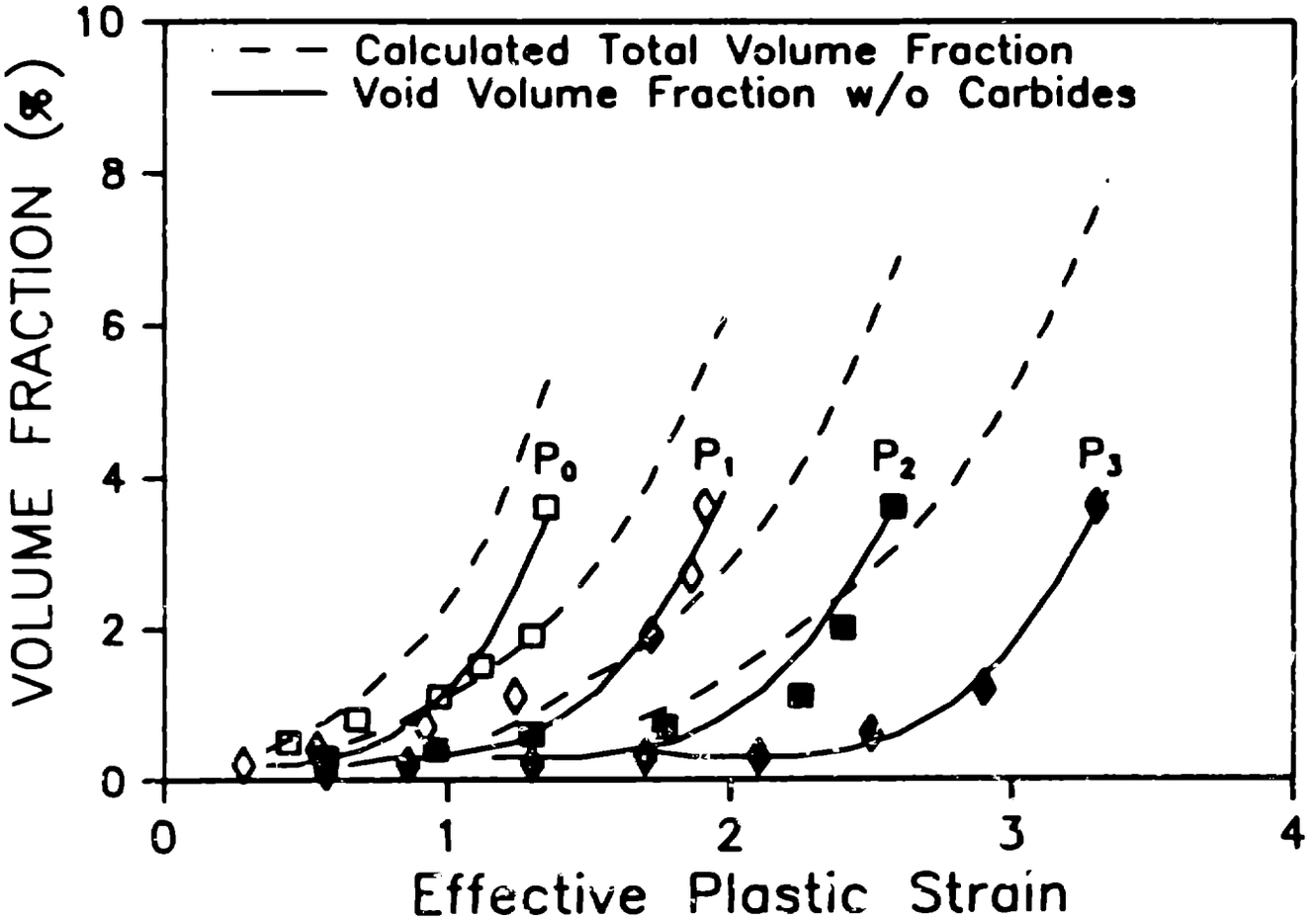

FIGURE 7 Plot of the calculated void volume fractions for each hydrostatic pressure compared to the experimental data from BrownRigg et al.

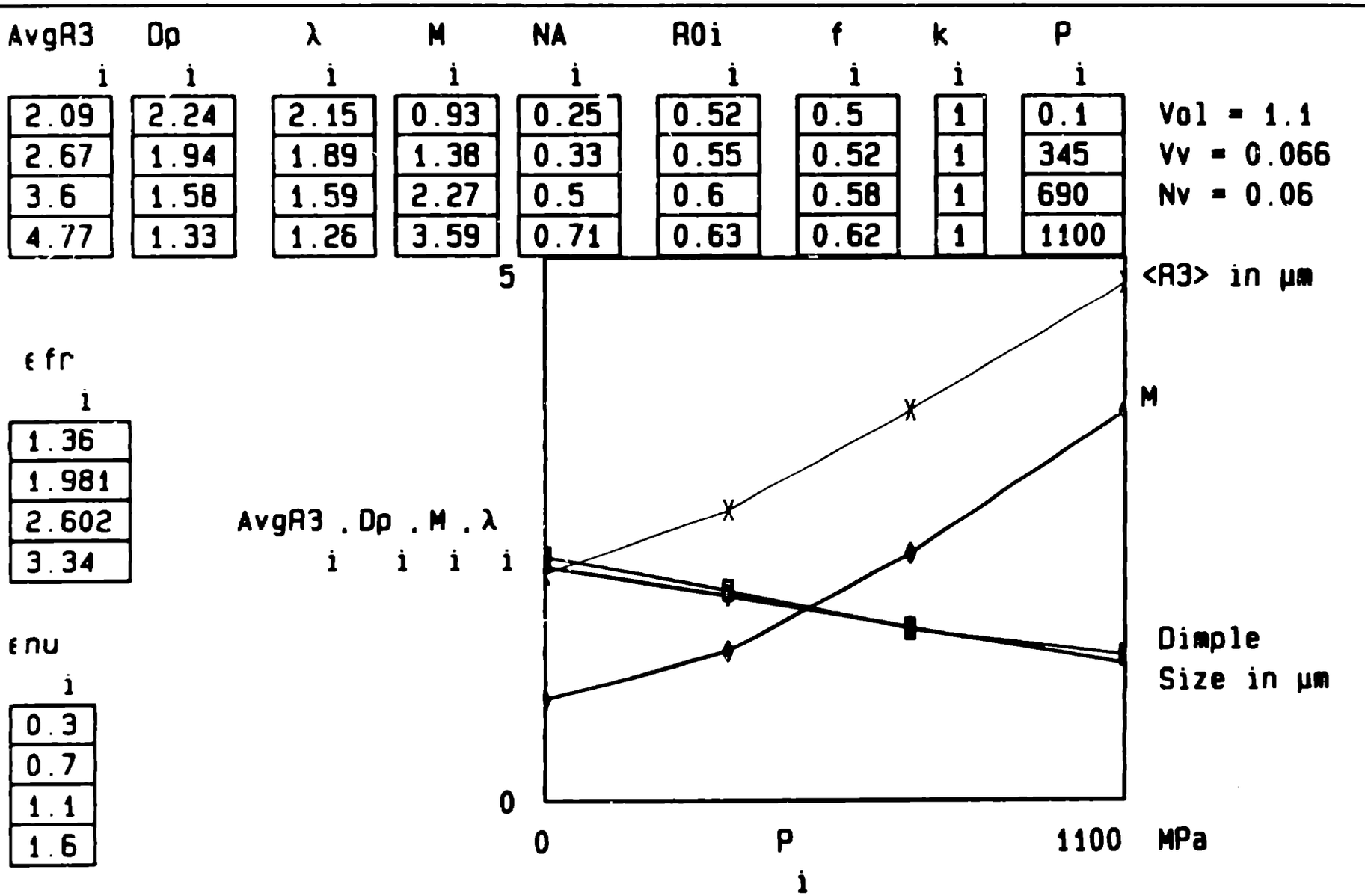

FIGURE 8 Plot of calculated values for <R3>, Dimple Size (Dp), and Microroughness (M), and Experimental Dimple Size (λ) vs Pressure

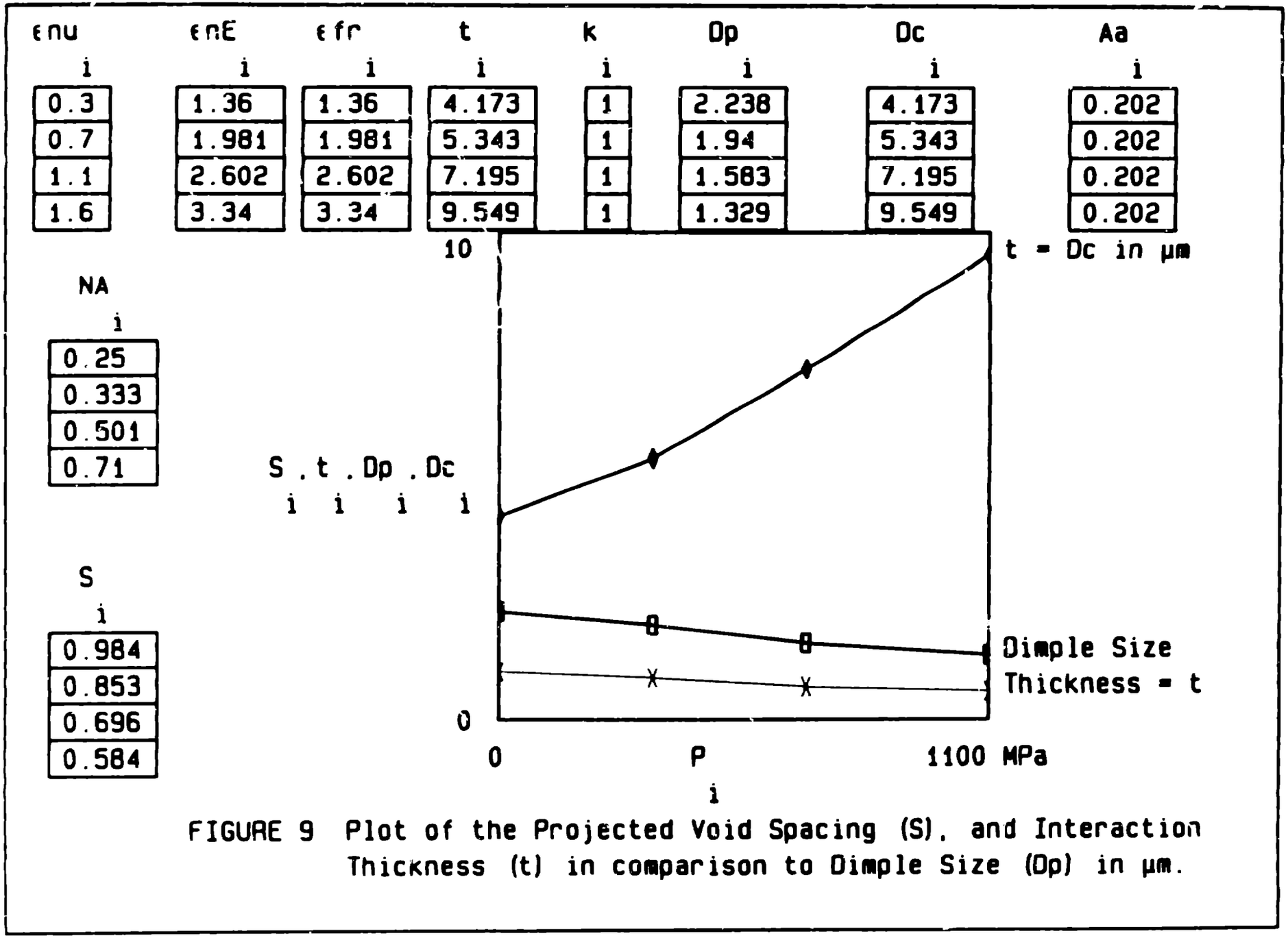

FIGURE 9 Plot of the Projected Void Spacing (S), and Interaction Thickness (t) in comparison to Dimple Size (Dp) in μm.

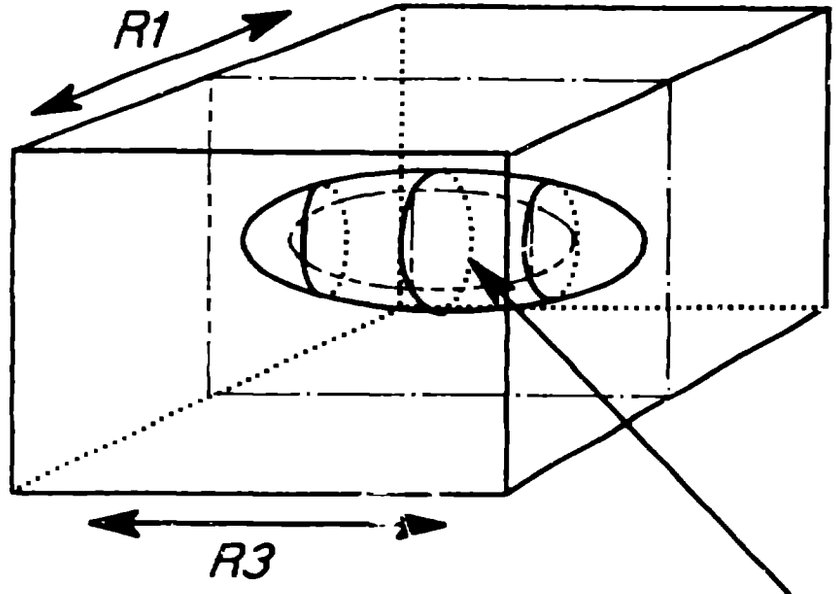

Diametral Circle of Prolate Ellipsoid

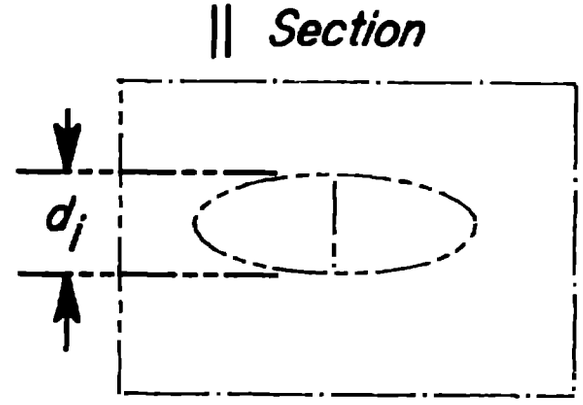

d_i = chord of diametral circle

Measure $\bar{Z}_{\parallel} = \overline{\left(\frac{1}{d_i}\right)}$

$$N_V \text{ (oriented particles)} = \frac{2}{\pi}\left(\bar{N}_{A\parallel}\right)\bar{Z}_{\parallel}$$

$$\bar{R1} = \frac{\pi}{4\bar{Z}_{\parallel}} \qquad \bar{R3} = \frac{\bar{N}_{A\perp}}{2N_V} = \frac{\pi}{4\bar{Z}_{\parallel}}\left[\frac{\bar{N}_{A\perp}}{\bar{N}_{A\parallel}}\right]$$

FIGURE 10 Estimation of Number in an Aggregate of Prolate Ellipsoids with Preferred Orientation.